

# Recovering Lost 21cm Radial Modes via Cosmic Tidal Reconstruction

Hong-Ming Zhu,<sup>1,2</sup> Ue-Li Pen,<sup>3,4,5,6</sup> Yu Yu,<sup>7</sup> and Xuelei Chen<sup>1,2,8</sup>

<sup>1</sup>Key Laboratory for Computational Astrophysics, National Astronomical Observatories,  
Chinese Academy of Sciences, 20A Datun Road, Beijing 100012, China

<sup>2</sup>University of Chinese Academy of Sciences, Beijing 100049, China

<sup>3</sup>Canadian Institute for Theoretical Astrophysics, 60 St. George Street, Toronto, Ontario M5S 3H8, Canada

<sup>4</sup>Canadian Institute for Advanced Research, CIFAR Program in Gravitation and Cosmology, Toronto, Ontario M5G 1Z8, Canada

<sup>5</sup>Perimeter Institute for Theoretical Physics, 31 Caroline St. N., Waterloo, ON, N2L 2Y5, Canada

<sup>6</sup>Dunlap Institute for Astronomy and Astrophysics, 50 St. George Street, Toronto, Ontario M5S 3H4, Canada

<sup>7</sup>Key laboratory for research in galaxies and cosmology, Shanghai Astronomical Observatory,  
Chinese Academy of Sciences, 80 Nandan Road, Shanghai 200030, China

<sup>8</sup>Center of High Energy Physics, Peking University, Beijing 100871, China

(Dated: April 25, 2016)

21 cm intensity mapping has emerged as a promising technique to map the large-scale structure of the Universe, at redshifts  $z$  from 1 to 10. Unfortunately, many of the key cross correlations with photo- $z$  galaxies and the CMB have been thought to be impossible due to foreground contamination for radial modes with small wavenumbers. These modes are usually subtracted in the foreground subtraction process. We recover the lost 21 cm radial modes via cosmic tidal reconstruction and find more than 60% cross-correlation signal at  $\ell \lesssim 100$  and even more on larger scales can be recovered from null. The tidal reconstruction method opens up a new set of possibilities to probe our Universe and is extremely valuable not only for 21 cm surveys but also for CMB and photometric redshift observations.

PACS numbers:

*Introduction.*—The current and future cosmological observations aim to map a large fraction of the Universe with unprecedented precision, varying from LSST [1], Euclid [2], Planck [3], CMB-S4 [4], and etc. In addition to these ones, 21 cm intensity mapping has emerged as a powerful probe of the cosmological large-scale structure [5, 6]. However, the astrophysical foregrounds from galactic and extra-galactic synchrotron and free-free emissions are stronger than the cosmological 21 cm signals by many orders of magnitude. These foregrounds are expected to be spectrally smooth, which means they would contaminate small radial modes, i.e., all modes with low  $k_{\parallel}$ . While there are not many modes with small  $k_{\parallel}$ , many other cosmic observations with broad window functions along the radial direction only probe these modes, such as weak lensing, photo- $z$  galaxies, integrated Sachs-Wolf effect, kinetic Sunyaev-Zel’dovich effect, and etc. Thus, the cross correlations of 21 cm surveys with these cosmic probes are dominated by foreground contamination [7, 8]. To solve this problem is of great importance for both 21 cm intensity mapping surveys and other key cosmic surveys.

Recently a new method called *cosmic tidal reconstruction* has been developed [9, 10]. It can reconstruct the large-scale tidal field and hence large-scale density field from the alignment of small-scale cosmic structures. The modes with small  $k_{\parallel}$  and large  $k_{\perp}$  are well reconstructed [10], which are exactly those lost in the foreground subtraction in 21 cm experiments. This technique enables the reconstruction of small radial modes, which provides important radial information essential for cross correlating with CMB and other cosmic probes.

In this Letter we study how to use cosmic tidal reconstruction to reconstruct the lost large-scale radial modes, and fur-

ther cross correlate with CMB lensing, photo- $z$  galaxies and ISW effect. We find such reconstruction technique recovers more than 60% cross-correlation signal at  $\ell \lesssim 100$  from nothing and even better on larger scales. This provides a new way to probe the origin and evolution of the Universe.

*Cosmic tidal reconstruction.*—Cosmic tides is a new way to view the tidal effect of gravity on the structure of matter clustering [9]. The large-scale density field can be reconstructed accurately from the anisotropic tidal distortions of the locally-measured matter power spectrum [9, 10]. The basic idea of purely transverse tidal reconstruction has been proposed in Ref. [9] and further expanded in Ref. [10]. Here, we briefly discuss the idea and summarize the process of cosmic tidal reconstruction.

The evolution of small-scale density perturbations is modulated by long-wavelength perturbations [11]. The anisotropic distortions in the local small-scale matter power spectrum,  $\propto \hat{k}^i \hat{k}^j t_{ij}^{(0)}$ , arise from the coupling of small-scale density fluctuations with the large-scale tidal field  $t_{ij}$ , where  $t_{ij} = \Phi_{L,ij} - \delta_{ij} \nabla^2 \Phi_L / 3$ ,  $\hat{\cdot}$  denotes the unit vector and superscript (0) denotes some “initial” time. The traceless tidal field  $t_{ij}$  can be decomposed into 5 independently observable components [10]. The two transverse shear terms,  $\gamma_1 = (\Phi_{L,11} - \Phi_{L,22})/2$  and  $\gamma_2 = \Phi_{L,12}$ , which describe quadrupolar distortions in the tangential plane perpendicular to the line of sight, are less affected by peculiar velocities and used to perform reconstruction [10]. The two gravitational tidal shear fields  $\gamma_1$  and  $\gamma_2$  can be converted to the two-dimensional (2D) convergence field,  $\kappa_{2D} = (\Phi_{L,11} + \Phi_{L,22})/2$ , using

$$\kappa_{2D,11} + \kappa_{2D,22} = (\gamma_{1,11} - \gamma_{1,22} + 2\gamma_{2,12}). \quad (1)$$

The three-dimensional (3D) convergence  $\kappa_{3D} = \nabla^2 \Phi_L / 3 \propto$

$\delta_L$ , which gives the large-scale density field, is given by

$$\kappa_{3D,11} + \kappa_{3D,22} = \frac{2}{3} \nabla^2 \kappa_{2D}. \quad (2)$$

Since only two transverse tidal shear fields  $\gamma_1(\mathbf{x})$  and  $\gamma_2(\mathbf{x})$  are used, the changes of the large-scale density field along the line of sight are inferred from the variations of  $\gamma_1$  and  $\gamma_2$  along the  $x_{\parallel}$  axis. The error of  $\kappa_{3D}$  is

$$\sigma_{\kappa_{3D}}(\mathbf{k}) \propto (k^2/k_{\perp}^2)^2, \quad (3)$$

which is anisotropic in  $k_{\perp}$  and  $k_{\parallel}$  [10]. The reconstruction works best for modes with low  $k_{\parallel}$  and high  $k_{\perp}$ , which can not be obtained from 21 cm surveys and contribute substantially to cosmological observables from other surveys mentioned above. Thus, cosmic tidal reconstruction provides a new way to recover the lost radial modes and to improve the cross correlations.

The tidal reconstruction works as follows. The first step is to convolve the density field with a Gaussian kernel,  $S(\mathbf{k}) = e^{-k^2 R^2/2}$ , which filters out the small-scale nonlinear structures. Here, we still take  $R = 1.25 \text{ Mpc}/h$  [9, 10]. The next step is to gaussianize the smoothed density field by taking a logarithmic transform or mapping the density fluctuations into a Gaussian distribution. In the following reconstructions, we adopt the latter method since after the simulated foreground subtraction, some of the density contrasts become smaller than  $-1$ , which makes it hard to take the logarithmic transform,  $\ln(1 + \delta)$ . The gravitational tidal shear fields can be estimated by applying quadratic tidal shear estimators  $\hat{\gamma}_1$  and  $\hat{\gamma}_2$  to the density field as in 21 cm lensing reconstruction [12]. Then the 3D tidal convergence field  $\kappa_{3D}$  is given by the linear combination of tidal shear fields using Eq. (1) and Eq. (2). The reconstructed noisy field  $\kappa_{3D}$  is related to the original density field as

$$\kappa_{3D}(k_{\perp}, k_{\parallel}) = b(k_{\perp}, k_{\parallel}) \delta(k_{\perp}, k_{\parallel}) + n(k_{\perp}, k_{\parallel}), \quad (4)$$

where  $b = P_{\kappa_{3D}}/P_{\delta}$  is the bias factor and  $n$  is the noise of reconstruction [10]. The reconstructed clean field is given by

$$\hat{\kappa}_c = (\kappa_{3D}/b)W, \quad (5)$$

where the Wiener filter  $W(k_{\perp}, k_{\parallel}) = P_{\delta}/(P_{\kappa_{3D}}/b^2)$ .

*Simulation setup.*—We further explore this idea with numerical simulations. We employ an ensemble of six  $N$ -body simulations from the CUBEP<sup>3</sup>M code [13]. Each simulation includes  $1024^3$  particles in a  $(1.2 \text{ Gpc}/h)^3$  box. In the following analysis we use outputs at  $z = 1$ .

We could approximately use dark matter to represent 21 cm source distributions. This is a good approximation since the neutral hydrogen traces the total mass distribution fairly well at low redshifts. We simply assume the experimental noise to be zero above a cut off scale and infinity below the cut off scale. This is a reasonable approximation for a filled aperture experiment, which has good brightness sensitivity and an exponentially growing noise at small scales. We choose this scale

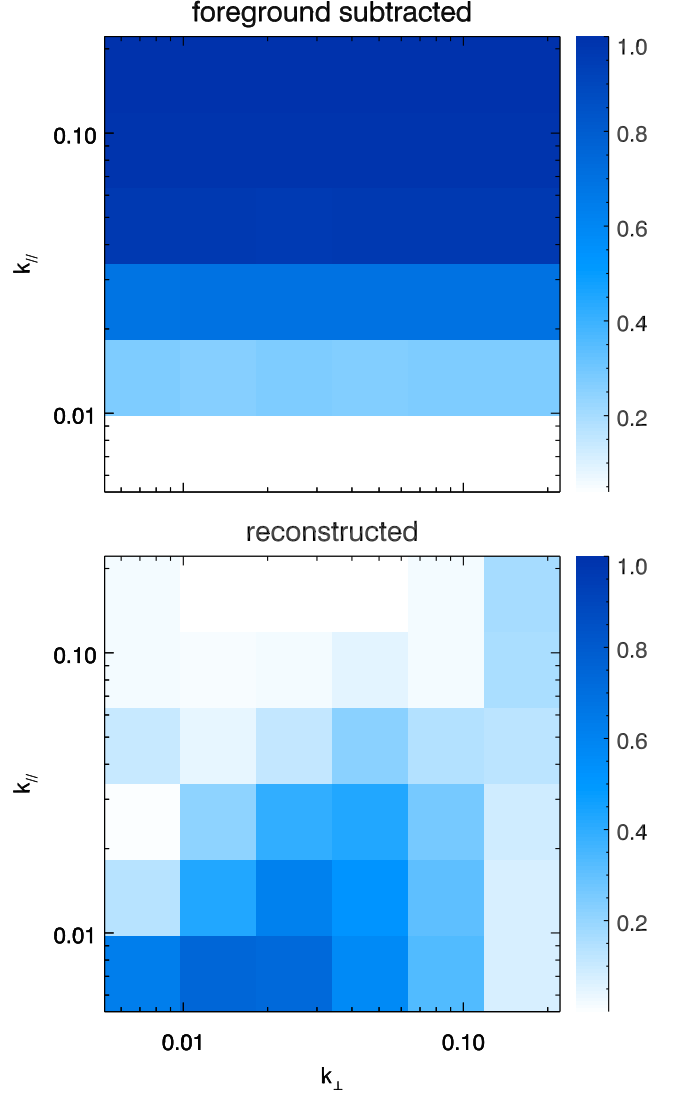


FIG. 1: (Top) The cross-correlation coefficient of the foreground subtracted density field with the original density field. (Bottom) The cross-correlation coefficient of the reconstructed field with the original density field. The lost radial modes appear again after reconstruction. The results are for  $R_{\parallel} = 60 \text{ Mpc}/h$  and  $k_c = 0.5 \text{ h}/\text{Mpc}$ .

to be  $k_c = 0.5 \text{ h}/\text{Mpc}$ , which corresponds to  $\ell = 1150$  at  $z = 1$ . This is realistic for the ongoing 21 cm experiments like CHIME [14], Tianlai [15], HIRAX [16], and etc.

We are not going to provide a detailed 21 cm data reduction process in this Letter, so we simply use a high-pass filter  $W_{fs}(k_{\parallel}) = 1 - e^{-k_{\parallel}^2 R_{\parallel}^2/2}$  to simulate the foreground subtraction. We show results for the two different scales  $R_{\parallel} = 60 \text{ Mpc}/h$  and  $R_{\parallel} = 15 \text{ Mpc}/h$ , which give  $W_{fs} = 0.5$  at  $k_{\parallel} = 0.02 \text{ Mpc}/h$  and  $k_{\parallel} = 0.08 \text{ Mpc}/h$ , respectively. The former is an optimal case, i.e., we remove modes for  $k_{\parallel} \lesssim 0.02 \text{ Mpc}/h$  while the latter is already achieved in the current 21 cm observations [17, 18].

The observed 21 cm field after foreground subtraction is

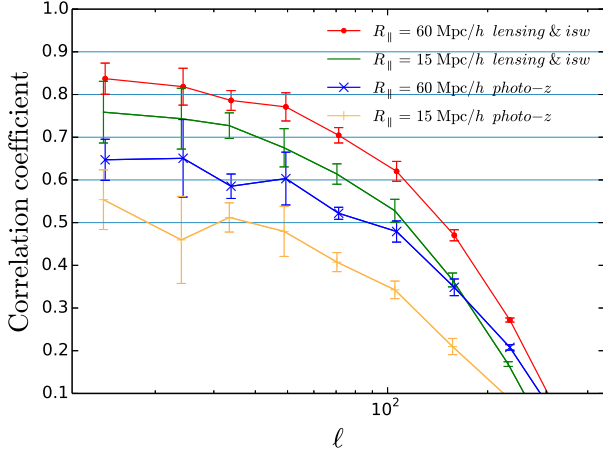


FIG. 2: The cross-correlation coefficients of 21 cm with different observations for both  $R_{\parallel} = 60$  Mpc/h and 15 Mpc/h with  $k_c = 0.5$  h/Mpc. Cosmic tidal reconstruction recovers about 60% signal at  $\ell \sim 100$  and much better results are obtained on larger scales. The error bars are estimated using the bootstrap resampling method.

given by

$$\delta_{fs}(\mathbf{k}) = \delta(\mathbf{k})W_{fs}(k_{\parallel})\Theta(k_c - k), \quad (6)$$

where  $\delta(\mathbf{k})$  is the density field from simulations,  $W_{fs}$  accounts the effect of foreground subtraction and  $\Theta(x)$  is the step function which equals 1 for  $x \geq 0$  and 0 otherwise. Then we get the reconstructed clean field  $\kappa_c$  from  $\delta_{fs}$  via cosmic tidal reconstruction. In Fig. 1, the upper panel shows the cross-correlation coefficient of  $\delta_{fs}$  with  $\delta$  and the lower panel shows the cross-correlation coefficient of  $\kappa_c$  with  $\delta$  for  $R_{\parallel} = 60$  Mpc/h. We find the lost radial modes appear again in the reconstructed field.

*Cross-correlation signals.*—To show how much the cross-correlation signal is recovered by cosmic tidal reconstruction and estimate the detectability of the cross correlation, we need to generate the lensing convergence field, the angular distribution of photo- $z$  galaxies and the temperature fluctuation due to the ISW effect using  $N$ -body simulations.

(1) CMB lensing.—The weak lensing convergence is a weighted projection of the dark matter density fluctuations along the line of sight to the last scattering surface,

$$\kappa(\boldsymbol{\theta}) = \int_0^{\chi_s} d\chi W_{\kappa}(\chi)\delta(\chi\boldsymbol{\theta}, \chi), \quad (7)$$

where the lensing kernel

$$W_{\kappa}(\chi) = \frac{3\Omega_{m0}H_0^2\chi(\chi_s - \chi)}{2a(\chi)\chi_s}, \quad (8)$$

with  $\chi_s = \chi(z_s = 1090)$ . To generate the convergence field from simulation data, we first squeeze the simulation box to a 2D plane, then multiply the  $W(\chi(z = 1))$ , as the lensing weight is a slowly varying function for the case of CMB lensing. Then we obtain the lensing convergence field contributed by the simulated density field.

(2) Photo- $z$  galaxies.—We calculate the projected galaxy density field at  $z \sim 1$  with usual photo- $z$  bin width of 0.2, i.e.,  $z_p \in (0.9, 1.1)$ . We adopt the galaxy distribution characterized by  $n(z) \propto z^{\alpha}\exp[-(z/z^*)^{\beta}]$  with  $\alpha = 2$ ,  $z^* = 0.5$ ,  $\beta = 1$  and assume the photo- $z$  scatter  $\mathcal{P}(z_p|z)$  is perfectly known to be in a Gaussian form with photo- $z$  error  $\sigma_z = 0.05(1+z)$ . The 2D angular galaxy distribution is given by

$$\delta_{2D}(\boldsymbol{\theta}) = \int_0^{\infty} dz W_p(z)\delta(\chi(z)\boldsymbol{\theta}, \chi(z)), \quad (9)$$

where the window function

$$W_p(z) \propto \int_{0.9}^{1.1} n(z)\mathcal{P}(z_p|z)dz_p \quad (10)$$

with normalization  $\int W_p(z)dz = 1$ .

(3) ISW effect.—The fractional CMB temperature fluctuations induced by the ISW effect is given as

$$\left(\frac{\Delta T}{T}\right)_{\text{ISW}}(\boldsymbol{\theta}) = -2 \int_0^{\chi_s} d\chi \frac{\partial \Phi(\chi\boldsymbol{\theta}, \chi)}{\partial \chi}. \quad (11)$$

In Fourier space, approximating that the evolution of  $\delta(\mathbf{k}, t)$  with time is given by linear theory  $\dot{\delta}(\mathbf{k}, t) = \dot{D}(t)\delta(\mathbf{k}, t=0)$ , we have

$$\frac{\partial \Phi(\mathbf{k}, \chi)}{\partial \chi} = -\frac{3\Omega_{m0}H_0^2}{2a(\chi)} \frac{\partial \ln(D/a)}{\partial \chi} \frac{\delta(\mathbf{k}, \chi)}{k^2}, \quad (12)$$

where  $D$  is the growth factor. In our implementation, we also approximate the time dependent factor as a constant across the simulation box.

In Fig. 2, we show the cross-correlation coefficients of 21 cm with different observations for both  $R_{\parallel} = 60$  Mpc/h and 15 Mpc/h. Due to the similar treatments of CMB lensing field and the ISW field, we get the same correlation coefficient for them. The correlation with photo- $z$  galaxies is smaller than the other two since we only use a narrow bin which locates at  $z = 1$  with bin width 0.2.

In each panel of Fig. 3, we show the cross-correlation signal  $C_{\ell}^{ij}$  and noise per mode  $(C_{\ell}^i n_{\ell}^j + n_{\ell}^i C_{\ell}^j + n_{\ell}^i n_{\ell}^j)^{1/2}$ , where  $n_{\ell}^i$  is the noise power spectrum. The error of the signal is

$$(\Delta C_{\ell}^{ij})^2 = \frac{1}{(2\ell+1)f_{\text{sky}}\Delta\ell} \left[ (C_{\ell}^{ij})^2 + (C_{\ell}^i + n_{\ell}^i)(C_{\ell}^j + n_{\ell}^j) \right] \quad (13)$$

For the 21 cm field,  $n_{\ell}^{21\text{cm}}$  is given through Eq. (5). The noise for CMB lensing is assumed to be the same as Planck 2015 results [19]. For photo- $z$  galaxies, the shot noise is negligible on degree scales. For ISW effect,  $n_{\ell}^{\text{ISW}}$  is the large-scale CMB power spectrum  $C_{\ell}^{TT}$ . We choose  $f_{\text{sky}}$  to be 0.25 for CMB lensing and photo- $z$  galaxies, and 1 for the ISW effect. By using cosmic tidal reconstruction, we are able to detect the cross-correlation signals with ongoing 21 cm experiments [14–16]. The redshift information contained in 21 cm observations allows us to constrain the expansion history of the Universe by cross correlating with the ISW effect. The detectability for

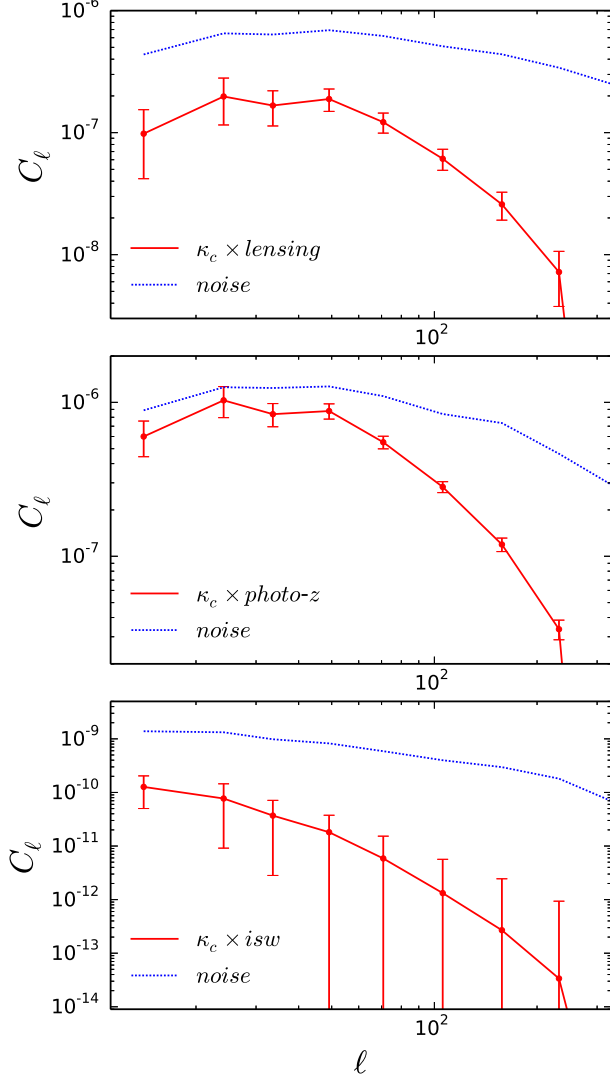


FIG. 3: (Top) The cross correlation of 21 cm and CMB lensing. (Middle) The correlation of 21 cm and photo- $z$  galaxies. (Bottom) The correlation of 21 cm and ISW effect. The solid curve shows the signal and the dotted curve shows the noise per mode. The results are for  $R_{\parallel} = 60$  Mpc/ $h$  and  $k_c = 0.5$   $h$ /Mpc.

ISW effect can be further improved by including CMB polarization data [20].

*Discussion.*—It may seem to be odd that the modes lost appear again after reconstruction. This can be understood intuitively. The reconstructed field  $\kappa_c$  is given by the linear combination of quadratic estimators, in the form of  $\kappa_c(\mathbf{x}) \sim \delta_{fs}(\mathbf{x})\delta_{fs}(\mathbf{x})$ . In Fourier space this can be written as  $\kappa_c(\mathbf{k}) \sim \int d^3k' \delta_{fs}(\mathbf{k}')\delta_{fs}(\mathbf{k} - \mathbf{k}')$ , i.e., the reconstructed field is given by the convolution of  $\delta_{fs}(\mathbf{k}')$  and  $\delta_{fs}(\mathbf{k} - \mathbf{k}')$ . Although  $\delta_{fs}$  has no small radial modes, i.e.  $k'_{\parallel}$  and  $k_{\parallel} - k'_{\parallel}$  can not be small,  $k_{\parallel}$  can reach the low  $k_{\parallel}$  regime. Here, we extract the information about matter distribution on large scales contained in the small-scale matter distributions. The power spectrum of  $\kappa_c$

is given by the connected four point function of  $\delta_{fs}$ , which means we are using the information that comes from higher order statistics and is not included in the two point statistics of  $\delta_{fs}$ , i.e., power spectrum.

The tidal shear estimators we used are optimal for Gaussian sources and in the long-wavelength limit [10]. The results can still be improved by constructing optimal tidal shear estimators for non-Gaussian sources as in 21 cm lensing [21] and constructing optimal estimators on all scales. This means here we present the “least optimal” case of recovering the cross-correlation signals and even better results can be achieved in future.

The BAO reconstruction technique [22] has been shown to be still useful in 21 cm surveys [23, 24]. While there are not many modes with small  $k_{\parallel}$  lost in the foreground subtraction, the differential motions which smear the BAO peaks are substantially contributed by large-scale modes with  $k \lesssim 0.1$   $h$ /Mpc [22]. The tidal reconstruction compensates the foreground wedge at low  $k_{\parallel}$  and high  $k_{\perp}$  and hence can further improve the BAO reconstruction in 21 cm surveys. All 21 cm experiments, no matter the low redshift experiments for BAO effect or the high redshift experiments for EOR signal, share the same foreground problem. Although not examined here, we expect great help from the cosmic tidal reconstruction in high redshift cross correlations, like 21 cm-kSZ signal from EOR [25]. Based on above discussions, we conclude that cosmic tidal reconstruction is extremely valuable for all cosmological 21 cm surveys as well as CMB and photometric redshift observations.

We acknowledge helpful discussions with Alex van Engelen, Marcelo Alvarez, Philippe Berger, Yi-Chao Li and Shifan Zuo. The simulations were performed on the BGQ supercomputer at the SciNet HPC Consortium. SciNet is funded by: the Canada Foundation for Innovation under the auspices of Compute Canada; the Government of Ontario; the Ontario Research Fund – Research Excellence; and the University of Toronto. We acknowledge the support of the Chinese MoST 863 program under Grant No. 2012AA121701, the CAS Science Strategic Priority Research Program XDB09000000, the NSFC under Grant No. 11373030 and 11403071, IAS at Tsinghua University, CHEP at Peking University, and NSERC. Research at the Perimeter Institute is supported by the Government of Canada through Industry Canada and by the Province of Ontario through the Ministry of Research & Innovation. The Dunlap Institute is funded through an endowment established by the David Dunlap family and the University of Toronto.

- 
- [1] P. A. Abell et al. (LSST Science Collaboration), ArXiv e-prints (2009), 0912.0201.
  - [2] L. Amendola, S. Appleby, D. Bacon, T. Baker, M. Baldi, N. Bartolo, A. Blanchard, C. Bonvin, S. Borgani, E. Branchini, et al., Living Reviews in Relativity **16**, 6 (2013), 1206.1225.

- [3] R. Adam et al. (Planck Collaboration), ArXiv e-prints (2015), 1502.01582.
- [4] W. L. K. Wu, J. Errard, C. Dvorkin, C. L. Kuo, A. T. Lee, P. McDonald, A. Slosar, and O. Zahn, *ApJ* **788**, 138 (2014), 1402.4108.
- [5] T.-C. Chang, U.-L. Pen, J. B. Peterson, and P. McDonald, *Physical Review Letters* **100**, 091303 (2008), 0709.3672.
- [6] T.-C. Chang, U.-L. Pen, K. Bandura, and J. B. Peterson, *Nature* **466**, 463 (2010), 1007.3709.
- [7] S. R. Furlanetto and A. Lidz, *ApJ* **660**, 1030 (2007), astro-ph/0611274.
- [8] P. J. Adshead and S. R. Furlanetto, *MNRAS* **384**, 291 (2008), 0706.3220.
- [9] U.-L. Pen, R. Sheth, J. Harnois-Déraps, X. Chen, and Z. Li, ArXiv e-prints (2012), 1202.5804.
- [10] H.-M. Zhu, U.-L. Pen, Y. Yu, X. Er, and X. Chen, arXiv e-prints (2015), 1511.04680.
- [11] F. Schmidt, E. Pajer, and M. Zaldarriaga, *Phys. Rev. D* **89**, 083507 (2014), 1312.5616.
- [12] T. Lu and U.-L. Pen, *MNRAS* **388**, 1819 (2008), 0710.1108.
- [13] J. Harnois-Déraps, U.-L. Pen, I. T. Iliev, H. Merz, J. D. Emberson, and V. Desjacques, *MNRAS* **436**, 540 (2013), 1208.5098.
- [14] K. Bandura et al., in *Society of Photo-Optical Instrumentation Engineers (SPIE) Conference Series* (2014), vol. 9145 of *Society of Photo-Optical Instrumentation Engineers (SPIE) Conference Series*, p. 22, 1406.2288.
- [15] Y. Xu, X. Wang, and X. Chen, *ApJ* **798**, 40 (2015), 1410.7794.
- [16] <http://www.acru.ukzn.ac.za/hirax/>.
- [17] K. W. Masui, E. R. Switzer, N. Banavar, K. Bandura, C. Blake, L.-M. Calin, T.-C. Chang, X. Chen, Y.-C. Li, Y.-W. Liao, et al., *ApJ* **763**, L20 (2013), 1208.0331.
- [18] E. R. Switzer, K. W. Masui, K. Bandura, L.-M. Calin, T.-C. Chang, X.-L. Chen, Y.-C. Li, Y.-W. Liao, A. Natarajan, U.-L. Pen, et al., *MNRAS* **434**, L46 (2013), 1304.3712.
- [19] P. A. R. Ade et al. (Planck Collaboration), ArXiv e-prints (2015), 1502.01591.
- [20] G.-C. Liu, K.-W. Ng, and U.-L. Pen, *Phys. Rev. D* **83**, 063001 (2011), 1010.0578.
- [21] T. Lu, U.-L. Pen, and O. Doré, *Phys. Rev. D* **81**, 123015 (2010), 0905.0499.
- [22] D. J. Eisenstein, H.-J. Seo, E. Sirko, and D. N. Spergel, *ApJ* **664**, 675 (2007), astro-ph/0604362.
- [23] H.-J. Seo and C. M. Hirata, *MNRAS* **456**, 3142 (2016), 1508.06503.
- [24] J. D. Cohn, M. White, T.-C. Chang, G. Holder, N. Padmanabhan, and O. Doré, *MNRAS* **457**, 2068 (2016), 1511.07377.
- [25] M. A. Alvarez, ArXiv e-prints (2015), 1511.02846.